Nuclear Engineering and Technology 54 (2022) 1126–1135

Contents lists available at ScienceDirect

Nuclear Engineering and Technology

journal homepage: www.elsevier.com/locate/net

Technical Note

Improvement of the subcooled boiling model for the prediction of the onset of flow instability in an upward rectangular channel

Adnan Wisudhaputra, Myeong Kwan Seo, Byong Jo Yun, Jae Jun Jeong*

School of Mechanical Engineering, Pusan National University, Busan, 46241, South Korea

ARTICLE INFO

Article history:
Received 26 July 2021
Received in revised form
3 September 2021
Accepted 12 September 2021
Available online 13 September 2021

Keywords:
Subcooled boiling
Onset of flow instability
Rectangular channel
The MARS code

ABSTRACT

The MARS code has been assessed for the prediction of onset of flow instability (OFI) in a vertical channel. For assessment, we built an experiment database that consists of experiments under various geometry and thermal-hydraulic condition. It covers pressure from 0.12 to 1.73 MPa; heat flux from 0.67 to 3.48 MW/m^2; inlet sub-cooling from 39 to 166 °C; hydraulic diameters between 2.37 and 6.45 mm of rectangular channels and pipes. It was shown that the MARS code can predict the OFI mass flux for pipes reasonably well. However, it could not predict the OFI in a rectangular channel well with a mean absolute percentage error of 8.77%. In the cases of rectangular channels, the error tends to depend on the hydraulic diameter. Because the OFI is directly related to the subcooled boiling in a flow channel, we suggest a modified subcooled boiling model for better prediction of OFI in a rectangular channel; the net vapor generation (NVG) model and the modified wall evaporation model were modified so that the effect of hydraulic diameter and heat flux can be accurately considered. The assessment of the modified model shows the prediction of OFI mass flux for rectangular channels is greatly improved.

1. Introduction

The occurrence of two-phase flow instabilities is not desirable in boiling, condensing, and other two-phase flow systems. The flow instabilities are divided into static instabilities and dynamic instabilities depending on the geometry of the flow, operating conditions, and boundary conditions. The Ledinegg instability or onset of flow instability (OFI) is an example of static instabilities in which flow undergoes a sudden, large-amplitude excursion to a new, stable operating condition. Such phenomena may cause mechanical vibration and generate premature boiling crisis or critical heat flux of the system, therefore, limiting the reliability and safety of the system's operation [1–5]. Considering the effect of the OFI, it is very important to predict the OFI point accurately.

The mechanism of OFI can be explained using Fig. 1. The dashed black line represents the supply curve determined from a certain pump characteristic and the black line represents the typical demand curve, which is also called the N-curve for a channel with given power input [6]. The OFI occurs when the slope of the external supply curve is greater than the demand curve. In the single-phase liquid region, the slope of the demand curve is greater than the slope of the supply curve, therefore, it is stable. When the mass flux decreases, the channel will reach the onset of nucleate boiling (ONB) point in which the first bubble is generated on the surface of the heating wall. Further decreasing in the mass flux, the channel will reach the net vapor generation (NVG) point. At this point, the bubbles represented by the red line start growing rapidly [7]. After the NVG point, if the mass flux decreases further, the channel reaches the OFI which is defined as the minimum pressure drop value in a decreasing mass flux system. The OFI is also used as the beginning of the unstable region [8].

In a research reactor that uses plate-type fuel, the fuel assemblies resemble a rectangular channel. Reactors that use this fuel type are Kijang Research Reactor (KJRR) [9] and many other examples [10–13]. It is noted that the OFI is not limited only to a pipe but covers all types of channel geometry [8]. Therefore, it is important to accurately predict the OFI in a rectangular channel. A study to assess the criteria to identify the OFI in an upward rectangular channel has already been done. Criteria based on the NVG, a part of the subcooled boiling model in thermal-hydraulic system code, is found to predict the OFI conservatively [14,15]. A study to assess the capability of RELAP5/3.2 [16] in parallel channels shows the influence of uncertainty related to the inlet sub-cooling, heat flux, and hydraulic diameter of the channel [17]. Another study

* Corresponding author.
E-mail address: jjjeong@pusan.ac.kr (J.J. Jeong).

https://doi.org/10.1016/j.net.2021.09.013

Nomenclature

A_{heat}	Heat transfer surface area (m^2)
c_{pf}	Specific heat capacity (J/kg K)
D_h	Hydraulic diameter (m)
G	Mass flux ($kg/m^2 \cdot s$)
h	Enthalpy (J/kg)
h_{fg}	Latent heat of vaporization (J/kg)
k	Thermal conductivity (W/m K)
Nu	Nusselt number
P	Pressure (Pa, bar)
Pe	Peclet number
q''	Heat flux (W/m^2)
T	Temperature (°C)
St	Stanton number
V	Volume (m^3)

Greek letters

α	Void fraction
ε	Error
Γ	Wall vapor generation rate per unit volume ($kg/m^3 \cdot s$)
ρ	Density (kg/m^3)

Subscripts

cr	Critical
f	Liquid phase
g	Gas phase
sat	Saturated
sub	Subcooled

aimed at simulating flow excursion by using the MARS code found that the MARS code provides reliable predictions and a rather conservative result [18].

This paper aims to improve the OFI prediction of the MARS code to extend its applicability for a reactor that uses plate-type nuclear fuel. The MARS code is assessed against several experiments at different thermal-hydraulic conditions and geometries. The result of the assessment is then used to propose a modified subcooled boiling model to improve the OFI prediction in an upward rectangular channel.

2. Assessment of the onset of flow instability prediction using the MARS code

The MARS-KS code is a best-estimate thermal-hydraulic system code developed by KAERI from the consolidated version of the RELAP5/MOD3.2 and COBRA-TF [19]. Since the backbone of the MARS-KS code is RELAP5 and COBRA-TF, the theoretical basis of the MARS code is very similar to those two codes except for the newly developed features, such as the multidimensional flow field formulation, the improved numerics for performance enhancement, and the coupled calculation features with 3D reactor kinetics and containment thermal-hydraulics [20].

2.1. Description of the subcooled boiling model in the MARS code

The subcooled boiling model in both RELAP5 and MARS is similar. It consists of the net vapor generation (NVG) model, wall evaporation model, interfacial condensation heat transfer et al. The NVG model determines the subcooled water temperature of NVG – later referred to as the point of net vapor generation (PNVG). The wall evaporation model determines the bubble generation rate on the surface of the heating wall. The interfacial condensation heat transfer determines the bubble condensation rate surrounded by subcooled liquid.

The original NVG model was developed by Saha-Zuber [21]. However, the Savannah River Laboratory (SRL) model [16] developed from the Saha-Zuber correlation has been used in most thermal-hydraulic codes including the RELAP5 code and the MARS code. The SRL model consists of the NVG model and the wall

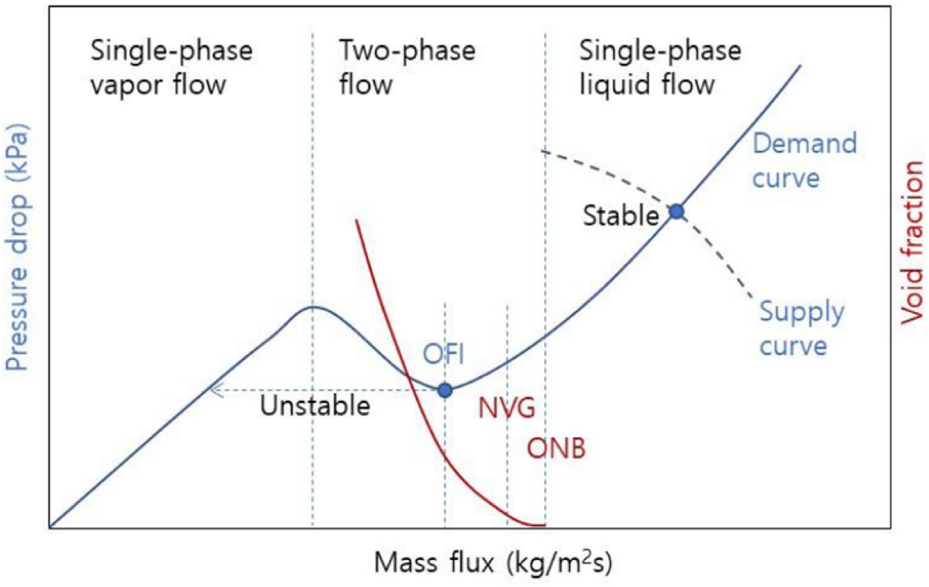

Fig. 1. Pressure-drop vs flow rate characteristic for a heated channel.

Table 1
OFI experiment database.

Experiment	Geometry	Diameter (mm)		Heat flux (MW/m^2)	Inlet sub-cooling (°C)	Pressure (bar)	Data points
		Gap (mm)	Width (mm)				
Whittle-Forgan 1 [8,22]	Rectangular	3.23	25.4	0.82–2.50	44–69	1.17	24
Whittle-Forgan 2 [8,22]		2.44	25.4	1.23–2.50	39–71	1.17–1.72	16
Whittle-Forgan 3 [8,22]		2.03	25.4	0.66–2.89	39–69	1.17	12
Whittle-Forgan 4 [8,22]		1.4	25.4	0.67–2.26	39–69	1.17	12
Vernier [24]		2	53.0	0.68–3.15	54–105	2.35	4
THTL 1 [23]		1.27	12.7	0.7–6.4	75–166	1.75–17	6
THTL 2 [23]		1.27	25.7	2.3–6.5	160–164	16.8–17.3	4
Whittle-Forgan 5 [8,22]	Pipe	6.45		0.86–3.48	39–59	1.17	9

evaporation model. The NVG model is represented as:

$$Nu = \frac{q'' D_h}{k_f (T_{sat} - T_{NVG})} = 455 \; for \; Pe \le 70,000, \tag{1a}$$

$$St = \frac{q''}{G c_{pf} (T_{sat} - T_{NVG})} = 0.0055 - 0.0009 F_{Press} \; for \; Pe > 70,000. \tag{1b}$$

Equations (1a) and (1b) can be rewritten as:

$$h_{cr} = \begin{cases} h_{f,sat} - \dfrac{1}{455} \dfrac{q'' c_{pf} D_h}{k_f} & \text{for } Pe \le 70,000, \\ h_{f,sat} - \dfrac{1}{0.0055 - 0.0009 F_{Press}} \dfrac{q''}{G} & \text{for } Pe > 70,000. \end{cases} \tag{2}$$

The wall evaporation model is given as follows:

$$\Gamma_w = \frac{q'' A_{heat}}{V h_{fg}} \left(\frac{1}{1 + \varepsilon_{SRL}} \right) (M + F_{SRL}), \tag{3}$$

where

$$M = \frac{\min\left(h_f, h_{f,sat}\right) - h_{cr}}{h_{f,sat} - h_{cr}}, \tag{4}$$

$$\varepsilon_{SRL} = \frac{\rho_f}{\rho_g} \frac{h_{f,sat} - \min\left(h_f, h_{f,sat}\right)}{h_{fg}} F_{eps}, \tag{5}$$

$$F_{SRL} = F_{\text{Press}} (F_{Gam} - M), \tag{6}$$

$$F_{Eps} = \min\left[1.0, \frac{1.0}{0.97 + 38.0 \times \exp\left[-\left(\frac{P}{6.894 \times 10^3} + 60 \right) \Big/ 42 \right]} \right], \tag{7}$$

$$F_{\text{Press}} = \frac{1.0782}{1.015 + \exp\left[\left(\frac{P}{6.894 \times 10^3} - 140.75 \right) \Big/ 28 \right]}, \tag{8}$$

$$F_{Gam} = \min\Big(1.0, 0.0022 + 0.11M - 0.59M^2 + 8.68M^3 - 11.29M^4 + 4.25M^5\Big). \tag{9}$$

The term M in the wall evaporation model is a function of h_{cr}, which is obtained from the NVG model. Therefore, the wall evaporation model is dependent on the NVG model.

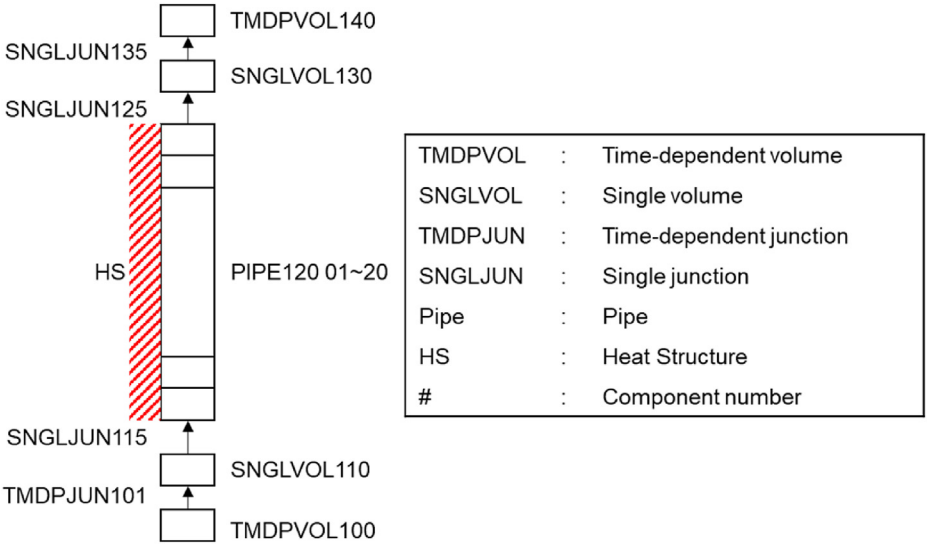

Fig. 2. Nodalization for OFI experiment in the MARS code.

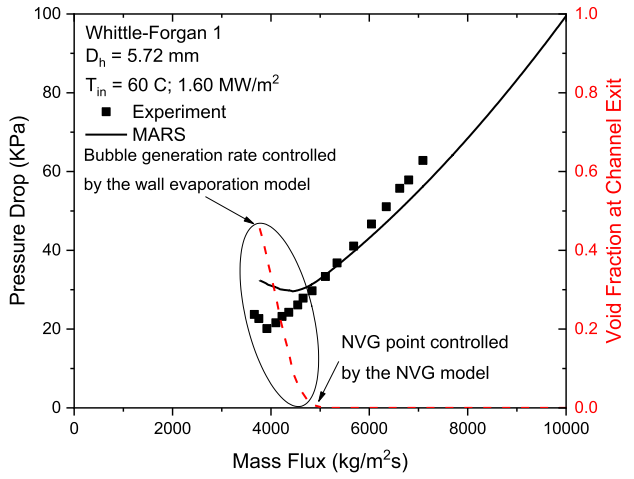

(a) Whittle-Forgan 1 [8, 22]

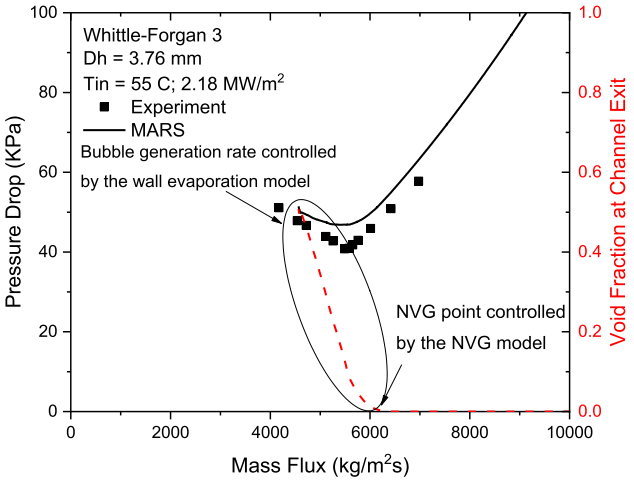

(b) Whittle-Forgan 3 [8,22]

Fig. 3. Pressure drop vs mass flux curve from the MARS code.

2.2. The OFI predictions of the MARS code

The MARS code is assessed against collected data of OFI experiments to improve its applicability on a narrow rectangular channel. The collected data mainly consists of upward flow experiments in a rectangular channel and a pipe. This includes the Whittle-Forgan [8,22], THTL [23], and Vernier [24] experiments. The details of the experiment are listed in Table 1.

The collected OFI experiments were simulated using the MARS code. The input model for the calculations is shown in Fig. 2. The component 100 is used to provide the boundary conditions of the inlet flow temperature. The component 101 is used to set the inlet flow rate. The component 120 represents the test section, where the heat structure components are attached to model the heat conduction and convective heat transfer to the liquid. The component 140 specifies the exit pressure. The component 110 and 130 represent the location of the pressure measurement taps. The channel pressure drop is calculated by using the pressure difference at the component 110 and 130.

For all the calculations, the heat flux provided is constant with the specified axial distribution. The mass flow rate is decreased in a stepwise function of time to produce a quasi-steady-state pressure drop vs. mass flux curve. The mass flow is kept constant for 20 s and then decreased for another 20 s until the next fixed flow rate. The

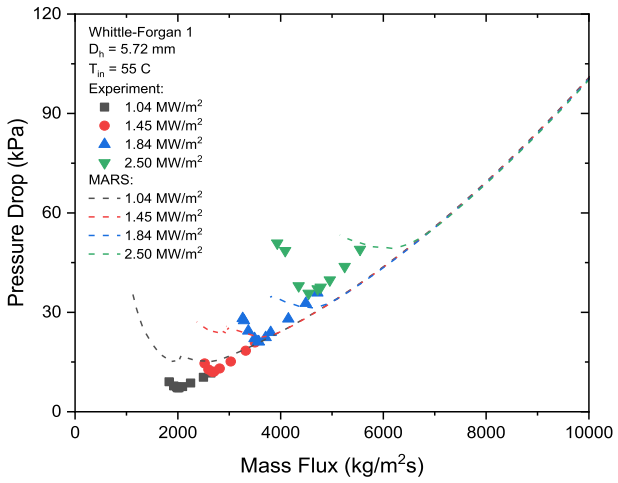

(a) Whittle-Forgan 1 [8, 22]

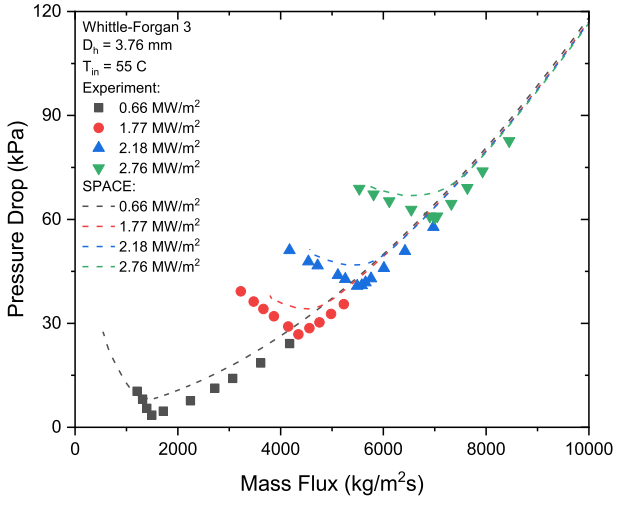

(b) Whittle Forgan 3 [8,22]

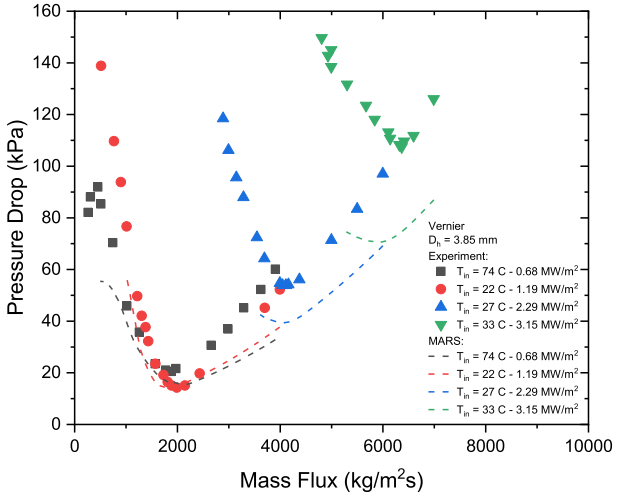

(c) Vernier [24]

Fig. 4. Comparison of the MARS results with the experiments.

Table 2
The MAPE of the OFI mass flux for the experiments.

Experiment	Geometry	Diameter (mm)		Hydraulic Diameter (mm)	Data Points	MAPE
		Gap (mm)	Width (mm)			
Whittle-Forgan 1 [8,22]	Rectangular	3.23	25.4	5.72	24	7.76%
Whittle-Forgan 2 [8,22]		2.44	25.4	4.45	16	10.34%
Whittle-Forgan 3 [8,22]		2.03	25.4	3.76	12	5.83%
Whittle-Forgan 4 [8,22]		1.4	25.4	2.65	12	6.95%
Vernier [24]		2	53.0	3.85	4	6.98%
THTL 1 [23]		1.27	12.7	2.37	6	18.14%
THTL 2 [23]		1.27	25.7	2.45	4	10.62%
Whittle-Forgan 5 [8,22]	Pipe	6.45		6.45	9	3.43%
Total	Include Pipe			2.37–6.45	87	8.22%
	Exclude Pipe			2.37–5.72	78	8.77%

calculation is kept running until it stopped either by the end of the time step or a code failure.

Fig. 3 shows examples of the pressure drop vs mass flux curve for OFI prediction in the MARS code. It can be seen that the PNVG always precedes the minimum pressure drop or the OFI point. It confirms that the NVG model is much more dominant for the OFI compared to the wall evaporation model. Fig. 4 shows some comparisons of the OFI in the experiment and the MARS calculation in different hydraulic diameters. The symbol indicates the experiment data and the line indicates the result from MARS calculation. The OFI point is taken as the point in which it has the minimum value of pressure drop. It can be seen that the OFI point is always over-predicted for Whittle-Forgan 1, generally acceptable for Whittle-Forgan 3, and acceptable for Vernier except for the high mass flux.

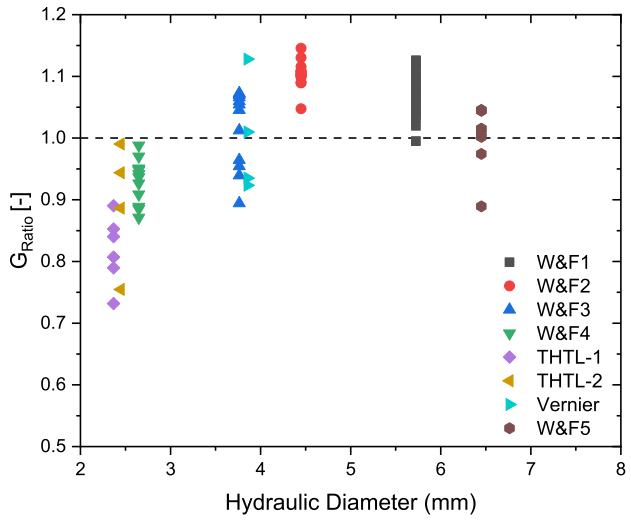

(a) Effect of hydraulic diameter

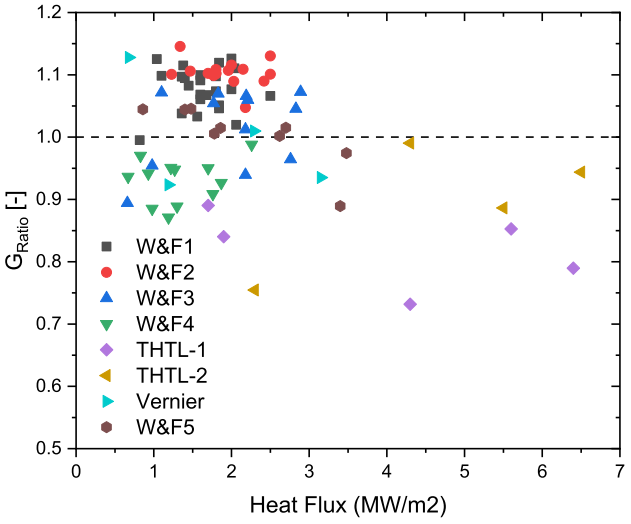

(b) Effect of heat flux

Fig. 5. The effects of hydraulic diameter and heat flux on the OFI prediction.

Quantitative evaluation is provided by the means of G_{Ratio} and mean absolute percentage error (MAPE). G_{Ratio} is defined as the ratio between OFI mass flux obtained from MARS calculation (G_{MARS}) to OFI mass flux from the experiment ($G_{Experiment}$):

$$G_{Ratio} = \frac{G_{MARS}}{G_{Experiment}}, \tag{10}$$

If G_{Ratio} is greater than one, the OFI is over-predicted while less than one means under-prediction. The MAPE is defined as:

$$MAPE = \frac{1}{N}\sum_{i=1}^{N}\left|\frac{G_{MARS,i} - G_{Experiment,i}}{G_{Experiment,i}}\right|. \tag{11}$$

Table 2 shows that the code can predict the OFI in a pipe reasonably well. However, the code failed to predict the OFI in a rectangular channel as it has average MAPE of 8.22%. The THTL 1 has the highest MAPE of 18.14%. It should be noted that this experiment has the smallest hydraulic diameter. In a study conducted by Hamidouche et al. [17], the hydraulic diameter has a significant influence in predicting the OFI point. Fig. 5(a) confirms it as the tendency of under-prediction at small hydraulic diameter, and over-prediction occurs at large hydraulic diameter up until it reached D_h = 4.5 mm in which the over-prediction is constant. Fig. 5(b) shows the effect of the heat flux on the OFI prediction. It could be seen that the code tends to under-predict the OFI mass flux at higher heat flux.

The NVG model in Eq. (1) is then plotted in Fig. 6(a), with the Peclet and Stanton number as the x-axis and y-axis, respectively. The Stanton number is evaluated at the channel exit. It shows the inability of the current model to predict the Stanton number for each experiment in a rectangular channel. The predicted Stanton number for the pipe is acceptable compared to the rectangular channel. Fig. 6(b) and Table 3 also show the effect of hydraulic diameter on the St-Pe relation. The average Stanton number tends to decrease as the hydraulic diameter gets smaller. The limiting criteria at Pe = 70,000 are also not suitable as the Stanton number for rectangular channel seems to be constant until a much lower Peclet number.

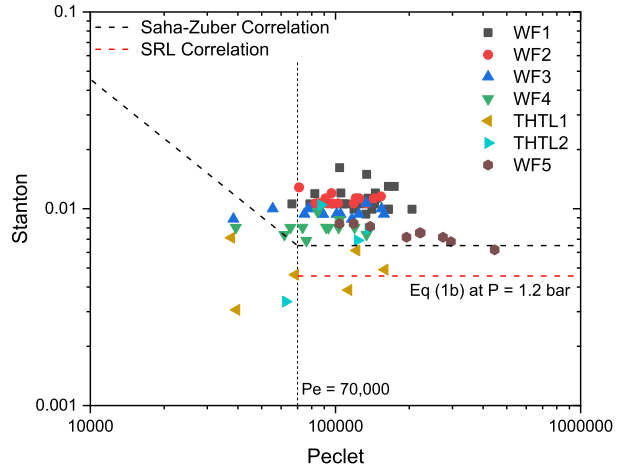

(a) St-Pe relation and the original NVG model

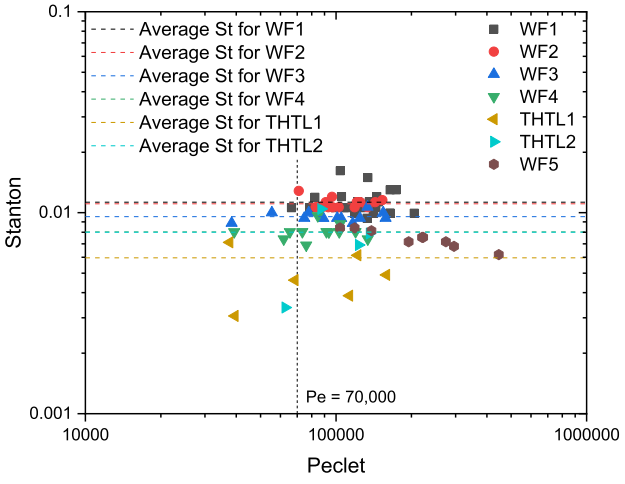

(b) The effect of hydraulic diameter on St-Pe relation

Fig. 6. Assessment of St-Pe relation.

In summary, the current model is only suitable for a pipe and not suitable for a rectangular channel. The current NVG model is not able to predict the Stanton number in a rectangular channel well as it does not take the effect of hydraulic diameter, and the limiting criteria at $Pe = 70{,}000$ also need to be changed. The code also tends to under-predict the OFI in high heat flux. Therefore, modification to the NVG model and the wall evaporation model is needed for better OFI prediction.

3. Improvement of the subcooled boiling model

Many studies aiming to improve the subcooled boiling model have been done [23,25–30]. The goal is to improve either the void fraction prediction or the OFI prediction. Some of these studies have opted to keep the Peclet number as the limiting criteria between the thermally controlled region and the hydrodynamically controlled region. However, the newer studies opted to develop a new correlation based on the equilibrium quality to obtain the PNVG. The limiting criteria are also changed based on the dimensionless inlet liquid velocity to divide between the low-velocity and high-velocity regions.

In this section, we proposed a modified NVG model and a modified wall evaporation model. The modified NVG model keeps the Peclet number as the limiting criteria between the thermally controlled region and the hydrodynamically controlled region.

3.1. Improvement of the NVG model

The original NVG model did not predict the Stanton number for the rectangular channel well while the Stanton number for the pipe is predicted reasonably well. It indicates that the original NVG model is suitable for the pipe while improvement needs to be done for the rectangular channel.

It is noted that, in the same flow area, the hydraulic diameter in a pipe will be larger compared to the hydraulic diameter in a rectangular channel. This in turn will cause the Stanton number in a rectangular channel to be bigger than the Stanton number in a pipe with the same flow area. Therefore, causing the PNVG in a rectangular channel to be generated in a lower sub-cooling temperature compared to the PNVG in a pipe. Ghione et al. [31] also mentioned that an enhancement of the heat transfer occurs with the decrease of the gap size which will cause the PNVG to be generated in much higher sub-cooling in a small hydraulic diameter. They also stated that the predictions of the Nusselt number are only accurate up to Re = 25,000 which in our experiment database corresponds to $Pe = 40{,}000$. Moreover, Fig. 6(b) shows that the Stanton number seems to be constant until around $Pe = 36{,}000$. It also shows that the Stanton number is decreasing as hydraulic diameter getting smaller. However, the original correlation used $Pe = 70{,}000$ as the limiting criteria to divide between the thermally controlled region (Peclet less than 70,000) and the hydrodynamically controlled region (Peclet greater than 70,000).

Therefore, we proposed a modification to the original model. We changed the limiting criteria to $Pe = 36{,}000$ and introduced the term D_{Rat}, which is a ratio between the test section's hydraulic diameter and a reference hydraulic diameter of 4.5 mm D_{Rat} will be used to decrease the Stanton number at a smaller hydraulic diameter which in turn will cause the PNVG to be generated in a higher sub-cooling. Then, the original model in Eq. (2) is modified as follows:

Table 3
Average Stanton number for each experiment.

Experiment	Geometry	Hydraulic Diameter (mm)	Average Stanton Number
Whittle-Forgan 1 [8,22]	Rectangular	5.72	0.01128
Whittle-Forgan 2 [8,22]		4.45	0.01108
Whittle-Forgan 3 [8,22]		3.76	0.00957
Whittle-Forgan 4 [8,22]		2.65	0.00803
THTL 1 [23]		2.37	0.00629
THTL 2 [23]		2.45	0.00732
Whittle-Forgan 5 [8,22]	Pipe	6.45	0.00748

$$h_{cr} = \begin{cases} h_{f,sat} - \dfrac{1}{399 \cdot D_{Rat}^{1.4}} \dfrac{q'' c_{pf} D_h}{k_f} & \text{for } Pe \le 36,000 \\ h_{f,sat} - \dfrac{1}{0.00834 - 0.00133 F_{Press}} \dfrac{q''}{G \cdot D_{Rat}^{1.4}} & \text{for } Pe > 36,000 \end{cases}, \quad (12)$$

where $D_{Rat} = \min\left(1.0, \frac{D_h}{0.0045}\right)$.

The comparison between the original and the modified NVG model is shown in Fig. 7. It can be seen that the over-predicted cases are greatly improved. The under-predicted case highlighted as (I) are not so improved. The result of Whittle-Forgan 5 with pipe highlighted as (II) deteriorates as the original NVG model is suitable for OFI prediction in a pipe. The under-predicted case generally has hydraulic diameters of less than 3.5 mm and heat flux greater than 3.0 MW/m^2.

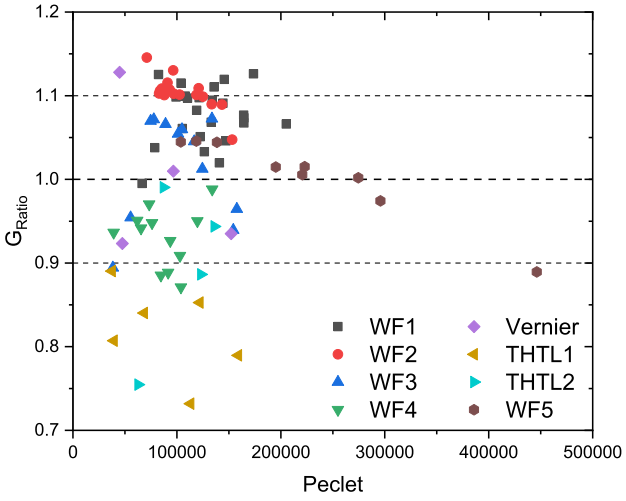

(a) The original NVG model

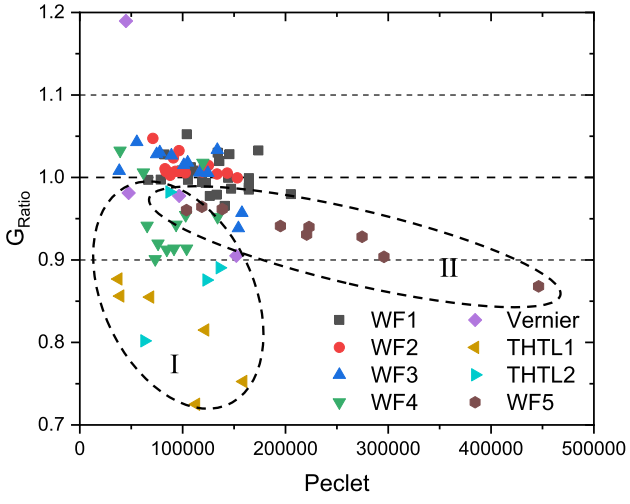

(b) The modified NVG model

Fig. 7. Comparison of the OFI prediction.

3.2. Improvement of wall evaporation model

The modified NVG model did not improve the under-predicted case. These consist of experiments with hydraulic diameters less than 3.5 mm and heat fluxes greater than 3.0 MW/m^2. The NVG point is now generated at a higher sub-cooling temperature in small hydraulic diameters. This will cause the bubble to be condensed again due to the high sub-cooling of the bulk temperature. As already mentioned, an enhancement of wall heat transfer occurs at a smaller gap size. We also assume that the superheated layer in which the bubble nucleation occurred has a higher effect in a channel with a small hydraulic diameter. The height of the superheated layer is difficult to obtain [32], however, Wiebe et al. [33] suggest that the region of high liquid superheat extends up to 0.254 mm. Liao et al. [34] pointed out that the thicker the height of the superheated layer, the faster the bubble grows. They also stated while higher heat flux decreases the superheated layer thickness due to enhanced turbulent convection, it also results in increased bubble generation, and the bulk liquid is stirred more rapidly by growing and departing vapor bubbles. Therefore, the wall evaporation model needs to be modified to consider the effect of the hydraulic diameter and heat flux.

In the wall evaporation model, F_{Gam} defined as Eq. (9) plays a key role in predicting the axial void fraction in low-pressure conditions [29]. The general form of F_{Gam} is shown in Fig. 8, and it did not consider the effect of hydraulic diameter and heat flux. Therefore, we proposed to modify the wall evaporation model which considers the effect of hydraulic diameter and heat flux. The modified wall evaporation model is written as:

$$F_{Gam} = \min\left[1.0, 0.0022 + 0.11M - 0.59M^2 + 8.68M^3 - 11.29M^4 + 4.25M^5 + 0.8121\left(df^{0.513} qf^{0.34}\right)\sin(\pi M)\right], \quad (13)$$

where $df = \max\left(1.0, \frac{0.0035}{D_h}\right) - 1$ and $qf = \max\left(1.0, \frac{q''}{3\times10^6}\right)$.

The term df is used to increase the bubble generation rate in a small hydraulic diameter (less than 3.5 mm) while the term qf is used to increase the bubble generation rate in large heat flux (more than 3.0 MW/m^2). The modification will change the form of F_{Gam} at different hydraulic diameters and heat fluxes as shown in Fig. 9.

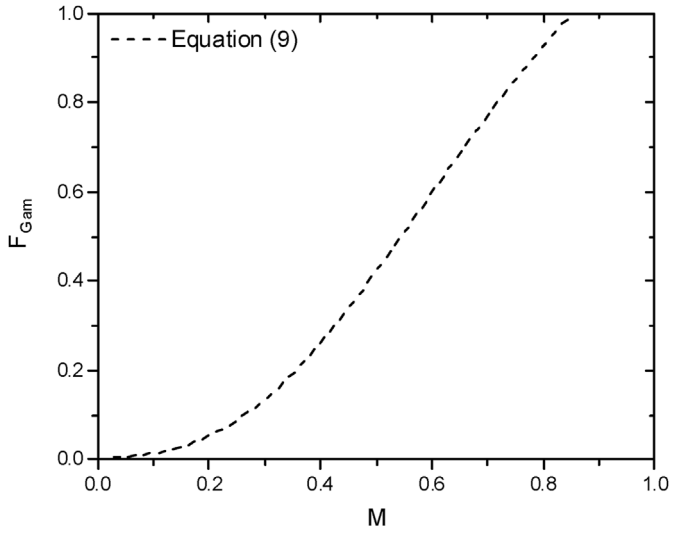

Fig. 8. The general form of F_{Gam}.

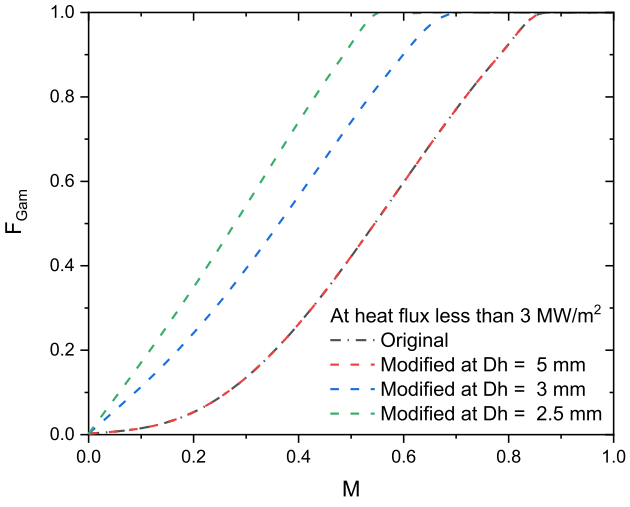

(a) At different hydraulic diameter

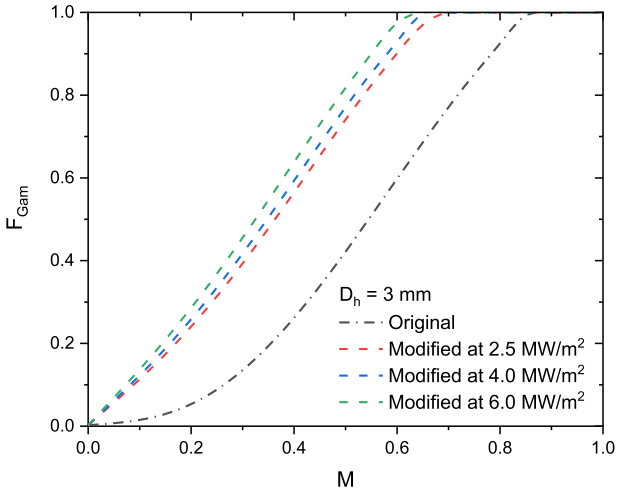

(b) At different heat flux

Fig. 9. The form of the modified F_{Gam}.

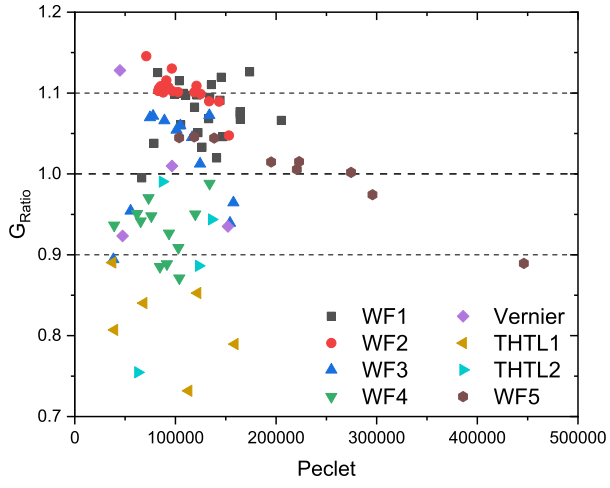

(a) The original model

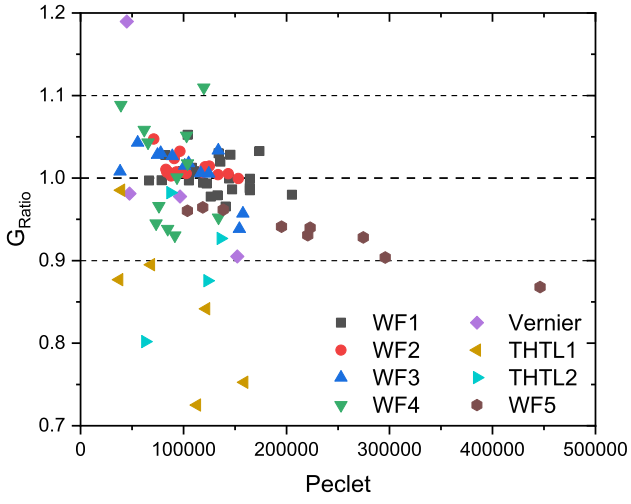

(b) The modified model

Fig. 10. Comparison between the original model and the modified model.

4. Assessment of the modified model

The modified subcooled boiling model is implemented to the MARS code and it is assessed with the same experimental database as those used to assess the original model. Also, we assessed the modified model with experiments that measured void fraction in a rectangular channel to ensure that the modified model doesn't deteriorate the original void fraction prediction.

4.1. Assessment of the OFI prediction

The comparison between the original and the modified model is shown in Fig. 10. The over-predicted case, such as the Whittle-Forgan 1, Whittle Forgan 2, Whittle Forgan 3, and Vernier, have been improved through the modification of the NVG model. The under-predicted case such as the Whittle-Forgan 4 is improved through the modification of the wall evaporation model. However, the OFI prediction for THTL 1 and THTL 2 is slightly improved. It shows the limitation of the modified model as it is unable to significantly improve the OFI prediction in a channel that has hydraulic diameter less than 2.5 mm. We assume that the friction factor has a more significant role in a channel with a very small hydraulic diameter. The OFI prediction for Whittle-Forgan 5 experiment is also deteriorated. This means that the modified model is not suitable for a pipe as explained in Section 3.1. Nevertheless, the OFI prediction is greatly improved as shown in Table 4, which provides the quantitative evaluation between the original and the modified model. It shows that the modified model greatly reduces the MAPE of the OFI prediction in a rectangular channel by 53.14%.

Table 4
Quantitative evaluation between the original and modified model.

Model	MAPE	
	All Experiment	Rectangular Channel
The original	8.22%	8.77%
The modified	4.37%	4.11%
Reduction of the MAPE	46.84%	53.14%

4.2. Assessment of void fraction prediction

To ensure that the modified model does not deteriorate the void

Table 5
Experiment database for the void fraction prediction.

Experiment	Gap (mm)	Width (mm)	Heat Flux (MW/m^2)	Inlet Sub-cooling (°C)	Pressure (bar)	Test No.	Data Points
Christensen [35]	11.1	44.4	0.21–0.50	1.2–14.4	27.6–68.9	7	112
Cook [36]	11.1	93.7	0.06–0.22	0.2–16.3	42.3–42.4	61	1066
Marchattere [37]	11.1	46.85–93.7	0.06–0.18	0.4–0.73	7.9–35.5	24	430
Marchattere [38]	6.35–12.7	50.8	0.01–0.27	1.7–19.4	11.2–42.4	141	1337

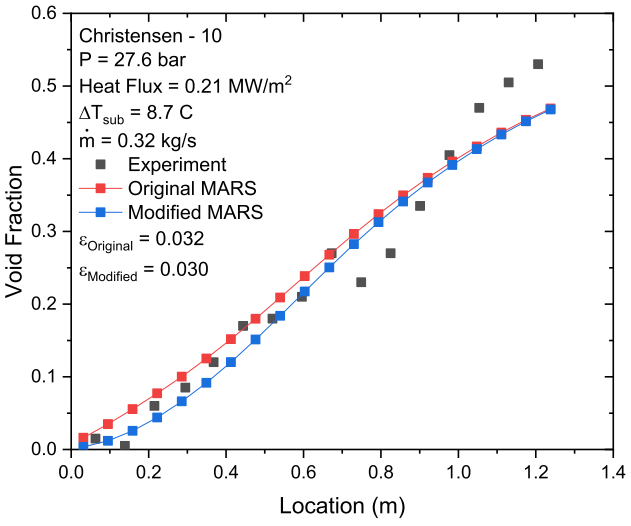

(a) Christensen

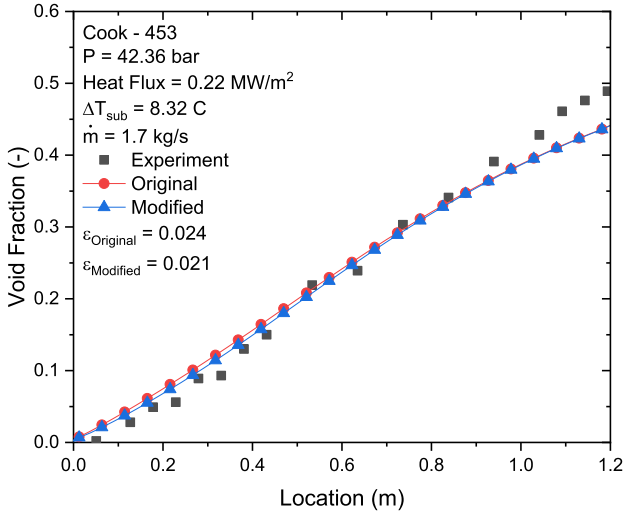

(b) Cook

Fig. 11. Comparison between the original and modified model.

fraction prediction, we have assessed the model against a void fraction experiment database. The experiment is designed to generate the NVG point near the channel inlet so that the void fraction distribution could be observed along the channel. The heat flux and mass flux in the experiment are kept constant. The experiment used to assess the void fraction prediction is listed in Table 5.

Fig. 11 shows the comparison between the original model and the modified model. The two results look similar each other. A quantitative comparison is provided in Table 6. The void fraction error (ε) is defined as

$$\varepsilon = \frac{1}{N}\sum_{i=1}^{N}\left|\alpha_{Experiment,i} - \alpha_{MARS,i}\right|, \tag{14}$$

where $\alpha_{Experiment,i}$ is the experiment void fraction at location i and $\alpha_{MARS,i}$ is the MARS void fraction at location i. The average error is reduced by 7%. Table 6 shows that the modified model has better prediction compared to the original model. Thus it can be said that the modified model managed to improve the void fraction prediction.

Table 6
Quantitative evaluation for the void fraction prediction.

Experiment	Test No.	Data Points	Average void fraction error	
			The original	The modified
Christensen [35]	7	112	0.0330	0.0322
Cook [36]	61	1066	0.0382	0.0380
Marchattere [37]	24	430	0.0210	0.0212
Marchattere [38]	141	1337	0.0490	0.0428
Total	233	2945	0.0404	0.0375
Reduction of the $\varepsilon_{Average}$			7.18%	

5. Conclusions

We have assessed the MARS code for the prediction of OFI using a total of 87 OFI experiments. It was shown that the MARS code did not predict the OFI point in a rectangular channel well. However, the OFI prediction for pipe is predicted reasonably well. It is because the MARS code did not consider the effect of hydraulic diameter and heat flux in a rectangular channel.

In this paper, we propose a modification to the subcooled boiling model since it is directly related to the OFI phenomena. We introduced correction factors that can consider the effects of hydraulic diameter and heat flux. The modified model is assessed again using the same experiment database. The modified model reduced the MAPE of OFI prediction from 8.77% to 4.11%. In addition, we also collected a total of 233 experiments to assess the effect of the modification to the void fraction prediction in a rectangular channel. The result showed that the modified model managed to improve the void fraction prediction in a rectangular channel. Therefore, the modified model can be used for the OFI prediction in a rectangular channel. The implementation of the modified model into MARS can extend the code applicability to the nuclear reactors that use a plate-type fuel.

Declaration of competing interest

The authors declare that they have no known competing financial interests or personal relationships that could have appeared to influence the work reported in this paper.

Acknowledgement

This research was partly supported by the National Research Foundation (NRF) of South Korea (Grant code 2019M2D2A1A03056998).

References

[1] J.A. Boure, A.E. Bergles, L.S. Tong, Review of two phase instabilities, Nucl. Eng. Des. 25 (1973) 165–192.
[2] L.C. Ruspini, C.P. Marcel, A. Clausse, Two-phase flow instabilities: a review, Int. J. Heat Mass Tran. 71 (2014) 521–548.
[3] M. Ishii, Study on Flow Instabilities in Two-phase Mixtures, Argonne National Laboratory, Argonne, 1976.
[4] M. Ledinegg, Instability of flow during natural and forced circulation, Die Wärme 61 (1938) 891–898.
[5] C.E. Brennen, Fundamentals of Multiphase Flows, Cambridge University Press, 2005.
[6] O.S. Al-Yahia, D. Jo, ONB, OSV, and OFI for subcooled flow boiling through a narrow rectangular channel heated on one-side, Int. J. Heat Mass Tran. 116 (2017) 136–151.
[7] G. Yadigaroglu, Two-phase flow instabilities and propagation phenomena, in: J.M. Delhaye, M. Giot, M.L. Riethmuller (Eds.), Thermohydraulics of Two-phase Systems for Industrial Design and Nuclear Engineering, vol. 2, McGraw-Hill, 1981.
[8] R.H. Whittle, R. Forgan, A correlation fo the minima in the pressure drop versus flow-rate curves for sub-cooled water flowing in a narrow heated channels, Nucl. Eng. Des. 6 (1967) 89–99.
[9] C.H. Seo, H.C. Kim, H.J. Park, H.T. Chae, Innovative design concepts for the KIJANG research reactor, in: Transactions of the Korean Nuclear Society Spring Meeting, 2013. Gwangju.
[10] S. Pinem, P.H. Liem, T.M. Sembiring, T. Surbakti, Fuel element burnup measurements for the equilibrium LEU silicide RSGGAS (MPR-30) core under a new fuel management strategy, Ann. Nucl. Energy 98 (2016) 211–217.
[11] Commissariat á l'Energue Atomique, Osiris Nuclear Reactors and Services Department, in: Commissariat Á l'Energue Atomique, 2008. Saclay.
[12] M.D. DeHart, Z. Karriem, M.A. Pope, M.P. Johnson, Fuel Element Design and Analysis for Potential LEU Conversion of the Advanced Test Reactor, Idaho National Laboratory, Idaho Falls, 2018.
[13] J.P. Dupuy, G. Perotto, G. Ithurralde, C. Leydier, X. Bravo, Jules Horowitz Reactor: general layout. main design options resulting from safety options, technical performances and operating constrains, in: TRTR-2005/IGORR-10 Joint Meeting, 2005. Gaithersburg.
[14] A. Ghione, B. Noel, P. Vinai, C. Demazière, Criteria for onset of flow instability in heated vertical narrow, Int. J. Heat Mass Tran. 105 (2017) 464–478.
[15] S.E.-D. El-Morshedy, Predictive study of the onset of flow instability in narrow vertical rectangular channels under low pressure subcooled boiling, Nucl. Eng. Des. 244 (2012) 34–42.
[16] The RELAP5-3D© Code Development Team, RELAP5-3D© Code Manual Volume I: Code Structure, System Models and Solution Methods, Idaho National Laboratory, Idaho Falls, 2005.
[17] T. Hamidouche, A. Bousbia-salah, RELAP5/3.2 assessment against low pressure onset of flow instability, Ann. Nucl. Energy 33 (2006) 510–520.
[18] C. Park, H.T. Chae, H. Kim, Simulation of flow excursion in a narrow flow channel by using the MARS code, in: Transactions of the Korean Nuclear Society Spring Meeting, 2007. Jeju.
[19] J.J. Jeong, K.S. Ha, B.D. Chung, W.J. Lee, Development of a multi-dimensional thermal-hydraulic system code, MARS 1.3.1, Ann. Nucl. Energy 26 (18) (1999) 1611–1642.
[20] KAERI, MARS Code Manual Volume I: Code Structure, System Models, and Solution Methods, KAERI/TR-2812/2004, Korea Atomic Energy Research Institute, 2007.
[21] P. Saha, N. Zuber, Point of net vapor generation and vapor void fraction in subcooled boiling, in: International Heat Transfer Conference, vol. 5, 1974. Tokyo.
[22] R. Forgan, R.H. Whittle, Pressure-drop Characteristics for the Flow of Subcooled Water at Atmospheric Pressure in Narrow Heated Channels, United Kingdom Atomic Energy Authority, Berkshire, 1966.
[23] M. Siman-Tov, D.K. Felde, J.L. McDuffee, J. Graydon L. Yoder, Static flow instability in subcooled flow boiling in parallel channels, in: 2nd International Conference on Multiphase Flow, Kyoto, 1995.
[24] S. Fabréga, J. Lafay, P. Vernier, Remarques sur la determination des echauffements critiques dans les reacteurs de recherche, in: Commissariat Á l'Energue Atomique, 1969. Saclay.
[25] V. Kalitvianski, Qualification of CATHARE 2 V1. 5 Rev. 6 on Subcooled Boiling Experiments (KIT Tests), CEA, Grenoble, 2000.
[26] K.S. Ha, Y.B. Lee, Improvements in predicting void fraction in subcooled boiling, Nucl. Technol. 150 (3) (2005) 283–292.
[27] T.-W. Ha, J.J. Jeong, B. Yun, H.Y. Yoon, Improvement of the MARS subcooled boiling model for low-pressure, low-Pe flow conditions, Ann. Nucl. Energy 120 (2018) 236–245.
[28] T.-W. Ha, J.J. Jeong, B.-J. Yun, Improvement of the MARS subcooled boiling model for vertical upward flow, Nucl. Eng. Technol. 51 (2019) 977–986.
[29] T.-W. Ha, B.-J. Yun, J.J. Jeong, Improvement of the subcooled boiling model for thermal-hydraulic system codes, Nucl. Eng. Des. 364 (2020).
[30] M.K. Seo, Improvement of the MARS Subcooled Boiling Model for the Prediction of OFI, Pusan National University, Busan, 2020.
[31] A. Ghione, B. Noel, P. Vinai, C. Demazière, Assessment of the thermal-hydraulic correlations for narrow rectangular channels with high heat flux and coolant velocity, Int. J. Heat Mass Tran. 99 (2016) 344–356.
[32] B.D. Marcus, D. Dropkin, Measured temperature profiles within the superheated boundary layer above a horizontal surface in saturated nucleate pool boiling of water, J. Heat Tran. 87 (3) (1965) 333–370.
[33] J.R. Wiebe, R.L. Judd, Superheat layer thickness measurements in saturated and subcooled nucleate boiling, J. Heat Tran. 93 (4) (1971) 455–461.
[34] J. Liao, R. Mei, J.F. Klausner, The influence of the bulk liquid thermal boundary layer on saturated nucleate boiling, Int. J. Heat Fluid Flow 25 (2004) 196–208.
[35] H. Christensen, Power-to-void Transfer Functions, Argonne National Laboratory, Argonne, 1961.
[36] W.H. Cook, Boiling Density in Vertical Rectangular Multichannel Sections with Natural Circulation, Argonne National Laboratory, Lemont, 1956.
[37] J.F. Marchattere, The Effect of Pressure in Boiling Density in Multiple Rectangular Channel, Argonne National Laboratory, Lemont, 1956.
[38] J.F. Marchattere, M. Petrick, P.A. Lottes, R.J. Weatherhead, W.S. Flinn, Natural and Forced Circulation Boiling Studies, Argonne National Laboratory, Argonne, 1960.